The Kinetics of Ca^{2+}-Dependent Switching in a Calmodulin−IQ Domain Complex†

D. J. Black, J. Eva Selfridge, and Anthony Persechini*

Division of Molecular Biology and Biochemistry, University of Missouri−Kansas City, Kansas City, Missouri 64110-2499

Received April 24, 2007; Revised Manuscript Received September 12, 2007

ABSTRACT: We have performed a kinetic analysis of Ca^{2+}-dependent switching in the complex between calmodulin (CaM) and the IQ domain from neuromodulin, and have developed detailed kinetic models for this process. Our results indicate that the affinity of the C-ter Ca^{2+}-binding sites in bound CaM is reduced due to a ∼10-fold decrease in the Ca^{2+} association rate, while the affinity of the N-ter Ca^{2+}-binding sites is increased due to a ∼3-fold decrease in the Ca^{2+} dissociation rate. Although the Ca^{2+}-free and Ca^{2+}-saturated forms of the CaM−IQ domain complex have identical affinities, CaM dissociates ∼100 times faster in the presence of Ca^{2+}. Furthermore, under these conditions CaM can be transferred to the CaM-binding domain from CaM kinase II via a ternary complex. These properties are consistent with the hypothesis that CaM bound to neuromodulin comprises a localized store that can be efficiently delivered to neuronal proteins in its Ca^{2+}-bound form in response to a Ca^{2+} signal.

At some level, all physiological responses involve coordinated biochemical changes triggered by intracellular Ca^{2+} signals. The Ca^{2+}-binding protein calmodulin (CaM[1]), which engages in modulatory interactions with more than 100 known target proteins, is the primary mediator of Ca^{2+}-dependent biochemical changes. Although many CaM targets, such as phosphodiesterase, myosin light chain kinase, and the constitutive nitric oxide synthases, do not interact significantly with the Ca^{2+}-free protein (*1*−*4*), a large class bind Ca^{2+}-free CaM at least as well as the Ca^{2+}-bound forms of the protein. The majority of these, including neuromodulin, neurogranin, the unconventional myosins, and some Ca^{2+}, K^+, and Na^+ channels, interact with CaM via IQ domains, which have the consensus sequence [I,L,V]QxxxR[G,x]xxx-[R,K] (*5*−*8*). These regions bind apoCaM and/or Ca^{2+}-bound CaM with dissociation constants ranging from subnanomolar to micromolar, depending upon their precise sequence and context (*6*). Complexes between CaM and IQ domains have been demonstrated to participate in a variety of regulatory processes, including positive and negative modulation of ion channels and unconventional myosin based motility (*6*). Some IQ domain proteins have been proposed to provide localized intracellular stores of CaM (*9*). The potential significance of such stores has been highlighted by recent investigations demonstrating that the intracellular CaM concentration can be limiting (*10*−*12*). Neuromodulin, a neuronal IQ domain protein found in axons and terminals, is perhaps the best studied example of such a protein (*9*). Neurogranin, a smaller protein with an essentially identical IQ domain, is thought to perform a similar function in dendritic spines (*13*, *14*).

The results presented in this paper indicate that the properties of the neuromodulin CaM−IQ domain complex promote dissociation of CaM in its Ca^{2+}-bound form, and allow it to be transferred to target proteins via a ternary complex. These features are conducive to the efficient delivery of Ca^{2+}-bound CaM to target proteins. Our results also demonstrate that the association rate constant for the C-ter EF pair of Ca^{2+}-binding sites in CaM is reduced by a factor of ∼10 in the IQ domain complex. This somewhat novel finding is consistent with the accompanying reduction in the affinity of the complex (*15*). The detailed kinetic models that we present for Ca^{2+}-dependent switching in this complex may be applicable to CaM−IQ domain complexes in proteins where Ca^{2+}-dependent switching appears to directly modulate function, such as ion channels and unconventional myosins (*5*−*8*).

MATERIALS AND METHODS

Proteins. The composition, expression, and purification of the fluorescent reporter, $BSCaM_{IQ}$, have been described in detail elsewhere (*15*), as have the methods used to express and purify native and mutant CaMs (*16*, *17*). The two mutant CaMs used in these studies are N_xCCaM, in which glutamic acid residues at positions 31 and 67 in the N-ter EF-hands have been replaced by alanines, and NC_xCaM, in which the homologous glutamic acid residues at positions 104 and 140

† This work was supported by NIH Grant GM074887 to A.P.

* To whom all correspondence should be addressed: Division of Molecular Biology and Biochemistry, University of Missouri−Kansas City, 5007 Rockhill Road, Kansas City, MO 64110-2499. Tel: 816-235-6076. Fax: 816-235-5595. E-mail: Persechinia@umkc.edu.

[1] Abbreviations: CaM, calmodulin; $BSCaM_{IQ}$, fluorescent biosensor containing a CaM-binding sequence based on the IQ domain in neuromodulin; ECFP, cyan emitting variant of green fluorescent protein, $EYFP_C$, yellow emitting variant of green fluorescent protein; N_xCCaM, mutant CaM with E31A and E67A substitutions; NC_xCaM, mutant CaM with E104A and E140A substitutions; N-ter, the NH_2-terminal end of a polypeptide; C-ter, the COOH-terminal end of a polypeptide; NC, Ca^{2+}-free CaM; N_2C, CaM with Ca^{2+} bound to both N-ter EF hands; NC_2, CaM with Ca^{2+} bound to both C-ter EF hands; N_2C_2, CaM with Ca^{2+} bound to all four EF hands; BAPTA, 1,2-bis(2-aminophenoxy)-ethane-*N*,*N*,*N*′,*N*′-tetraacetic acid; dibromo-BAPTA, 1,2-bis(2-amino-5,5′-dibromophenoxy)ethane-*N*,*N*,*N*′,*N*′-tetraacetic acid; FRET, fluorescence resonance energy transfer; ckPEP, a synthetic peptide based on the CaM-binding domain in CaM-dependent protein kinase II; ngPEP, a synthetic peptide based on the CaM-binding domain in neurogranin.

10.1021/bi700774s CCC: $37.00
Published on Web 10/24/2007

have been replaced. As designated by the "x" subscript, these mutations eliminate Ca^{2+} binding to the N-ter or C-ter EF hand pair. Two synthetic peptides were used in these studies. One, termed ckPEP, is based on the CaM-binding domain in CaM-dependent protein kinase II and has the sequence MHRQETVDCLKKFNARRKLKGAILTTMLA (Calbiochem, San Diego, CA). The other, termed ngPEP, is based on the IQ domain in neurogranin and has the sequence AAKIQASFRGHMARKK (Promega, Madison, WI).

Stopped-Flow Fluorescence Measurements. All dynamic fluorescence measurements were performed using an SX18-MV Stopped-Flow Reaction Analyzer with a nominal ~1.4 ms dead time (Applied Photophysics, Leatherhead, U.K.). Excitation light from a 75 W xenon arc lamp is supplied via a fiber-optic-coupled monochromator (5 nm slit widths). Fluorescence emission is monitored using a high voltage PMT fitted with an appropriate absorbance filter. To monitor changes in FRET between ECFP and $EYFP_C$ in $BSCaM_{IQ}$, ECFP fluorescence was excited at 430 nm and $EYFP_C$ emission was monitored using an LG535 long-pass absorbance filter (Corion, Franklin, MA). Ca^{2+}-dependent changes in quin-2 fluorescence excited at 330 nm were monitored using an LG505 long-pass emission filter. In experiments where quin-2 or CaM-binding peptides were used to trap Ca^{2+} or CaM, a range of quin-2 or peptide concentrations were examined to ensure the absence of rebinding. All progress curves presented are the average of at least 6 individual determinations. Reactions were initiated by rapidly mixing equal volumes of reactant solutions to produce the stated final reactant concentrations. The base experimental buffer contained 25 mM Tris, pH 7.5, 0.1 M KCl, and100 μg/mL BSA, with other components as specified in the text or captions. Where indicated, proteins and buffers were decalcified by successive treatments with Chelex and a BAPTA-polystyrene column (Molecular Probes, Inc.). Contaminating amounts of Ca^{2+} in decalcified protein solutions were 50 nM or less, based on the absence of any detectible effect on the A_{263} of BAPTA. Stopped-flow experiments were performed at 22 °C.

Analysis and Modeling of Kinetic Data. Rate constants were derived from fits of individual fluorescence time courses to single or double exponentials or from global fits of multiple time courses to explicit kinetic models performed using the Dynafit program (*18*). Standard errors given for the fitted parameters are the square roots of the diagonal elements in the variance−covariance matrices calculated for the nonlinear least-squares fits. In order to perform global fitting to explicit models it was necessary to assign relative molar fluorescence amplitudes to all kinetic species so as to account for their contributions to observed fluorescence. Values of 1.0 and 0.68 were assigned to free $BSCaM_{IQ}$ and the Ca^{2+}-free CaM−$BSCaM_{IQ}$ complex, and values of 0.83 and 0.85 were assigned to the Ca^{2+}-saturated complex and the intermediate complexes in which one CaM EF hand pair or the other is Ca^{2+}-saturated. These values were previously determined under equilibrium conditions, and were validated in the stopped-flow fluorometer (*15*). Occupancy of an EF hand pair by only a single Ca^{2+} ion was assumed to have no effect on fluorescence, because fluorescence changes observed under equilibrium conditions appear to require occupancy of both Ca^{2+}-binding sites (*15*).

Scheme 1

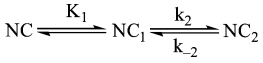

Ca^{2+} Association and Dissociation. We have modeled Ca^{2+} binding to each EF hand pair in CaM according to a sequential model, as illustrated by Scheme 1. By convention, the two Ca^{2+}-binding steps corresponding with occupancy of the C-ter EF hand pair are numbered 1 and 2 (as in Scheme 1), while the two N-ter Ca^{2+}-binding steps are numbered 3 and 4. A sequential Ca^{2+} binding model is the simplest one that accounts for the fact that dissociation of both Ca^{2+} ions from an EF hand pair is always observed to occur with a single apparent rate (*19*, *20*). The trivial explanation that Ca^{2+} dissociates independently from both sites at the same rate is inconsistent with the high degree of binding cooperativity (*19*). It is also inconsistent with ^{15}N spin relaxation experiments, which indicate that the second Ca^{2+} release step is at least 100 times faster than the first (*21*). Since the second Ca^{2+} ion is released much faster than the first, we also treat the first Ca^{2+} binding step as rapidly equilibrating. This assumption becomes invalid at free Ca^{2+} concentrations where $k_2[Ca^{2+}] \approx k_{-1}$ or $k_4[Ca^{2+}] \approx k_{-3}$, but it appears to be applicable over the range of Ca^{2+} concentrations used in these investigations.

Scheme 2

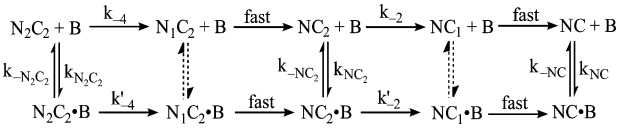

The Transition from Ca^{2+}-Saturated to Ca^{2+}-Free Complex. The data presented in Figure 4 were globally fitted to the kinetic model given in Scheme 2. In this scheme, B corresponds with $BSCaM_{IQ}$, NC corresponds with Ca^{2+}-free CaM, and N_2C_2 corresponds with CaM in which both the N-ter (N) and C-ter (C) EF hand pairs are replete with Ca^{2+}. Intermediate Ca^{2+}-bound states are designated appropriately. Since Ca^{2+} dissociates much more rapidly from the N-ter EF hand pair than it does from the C-ter pair, dissociation of Ca^{2+} is treated as a sequential process, with the N-ter pair of sites going first. The vertical dashed arrows denote steps that were omitted from fitting calculations because dissociation of the second Ca^{2+} ion from an EF hand pair is assumed to be much faster than dissociation of $BSCaM_{IQ}$. "Fast" rate constants were arbitrarily assigned values 10-fold larger than the rate constants preceding them.

Release of $BSCaM_{IQ}$ after Addition of $Ca^{2+}$and ckPEP. The data presented in Figure 5 were globally fitted according to the model given in Scheme 3. In this scheme, P corresponds with a peptide (ckPEP) based on the CaM-binding domain in CaM kinase II. Since the peptide prevents reassociation of CaM, rate constants for reversal of the second C-ter Ca^{2+}-binding step (k_{-2} and k'_{-2} can be omitted because the rate constants for dissociation of the CaM complex (k_{-NC_2} and $k^{T}_{N_2C_2}$) are much larger (see Tables 1 and 2). Dissociation of the Ca^{2+}-free complex can also be ignored, as it occurs at a rate of ~1 s^{-1}, which is far slower than the Ca^{2+} dissociation steps. Since the dissociation rate

Scheme 3

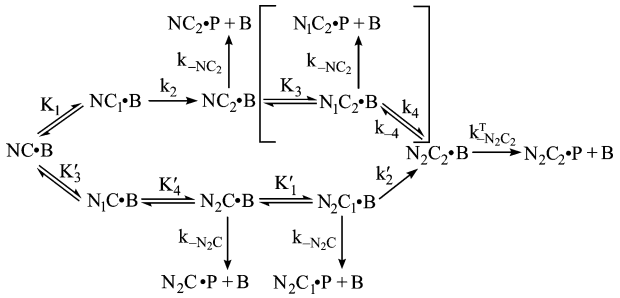

constant for the N_2C-B complex (k_{N_2C}) is much smaller than k'_{-4} (see Tables 1 and 2), we can treat both N-ter Ca^{2+}-binding steps on the lower pathway in the scheme as rapidly equilibrating, with dissociation constants of K'_3, K'_4. This approach is not applicable to the N-ter Ca^{2+}-binding steps on the upper pathway because the apparent Ca^{2+} dissociation rate constant for the N-ter sites (k_{-4}) is similar to the rate for dissociation of a presumptive peptide ternary complex ($k^{T}_{N_2C_2}$; see Tables 1 and 2). However, this is not a significant issue because the bracketed steps can be omitted from fitting calculations without significantly affecting the fit or the derived parameter values. The probable basis for this is explained in Results.

RESULTS

Association of CaM and BSCaM$_{IQ}$. The first step in these investigations was to derive apparent association and dissociation rate constants (k_{on} and k_{off}) for the various complexes between native or mutant CaM and $BSCaM_{IQ}$, a fluorescent reporter containing the IQ domain from neuromodulin (*15*). This was accomplished by determining observed association rates (k_{obs}) under pseudo-first-order conditions at a series of different CaM concentrations. Values for k_{on} and k_{off} were then derived from linear least-squares fits to replots of k_{obs} *vs* [CaM]. Values for k_{on} and k_{off} of $3.6 \pm 0.2 \times 10^5$ M^{-1} s^{-1} and 0.9 ± 0.2 s^{-1} were derived for the Ca^{2+}-free native CaM complex from the replot presented in Figure 1A. The k_{off}/k_{on} ratio of 2.5 ± 0.6 μM calculated for this complex is essentially identical to the equilibrium K_d value of 2.3 ± 0.1 μM (Table 1). Similar rate constants were derived for the Ca^{2+}-free N_xCCaM and NC_xCaM complexes (Table 1; data not shown). Values for k_{on} and k_{off} of $1.1 \pm 0.2 \times 10^6$ M^{-1} s^{-1} and 30.9 ± 1.6 s^{-1} were derived for the Ca^{2+}-saturated NC_xCaM complex from the replot in Figure 1B, and the k_{off}/k_{on} ratio of 28.1 ± 5.3 μM calculated for this complex agrees well with the equilibrium K_d value of 36.7 ± 3.9 μM (Table 1). Values for k_{on} and k_{off} of $3.1 \pm 0.2 \times 10^7$ M^{-1} s^{-1} and 69.4 ± 9.6 s^{-1} were derived for the Ca^{2+}-saturated complex with native CaM from the replot in Figure 1C; and respective values of $4.1 \pm 0.2 \times 10^7$ M^{-1} s^{-1} and 558.8 ± 10.1 s^{-1} were derived for the Ca^{2+}-saturated N_xCCaM complex from the replot in Figure 1D. The k_{off}/k_{on} ratios of 2.2 ± 0.3 and 13.6 ± 1.1 μM calculated for these complexes are essentially identical to their equilibrium K_d values of 2.5 ± 0.1 and 14.4 ± 1.3 μM (Table 1). The overall agreement between k_{off}/k_{on} ratios and equilibrium K_d values confirms that CaM binding to the neuromodulin IQ domain is a simple bimolecular process. Occupancy of one or both EF hand pairs in CaM significantly accelerates binding kinetics, although the greatest effect is seen when the C-ter EF hand pair is occupied. The accelerated rates observed in the presence of Ca^{2+} may serve to mobilize neuromodulin-bound CaM in response to a Ca^{2+} signal. The association rate constants for the CaM−IQ domain complexes in which the C-ter EF hand pair is Ca^{2+} bound are similar to those for the complexes between CaM and canonical target proteins, such as myosin light chain kinase or nitric oxide synthase (*22*, *23*). In contrast, the association rates derived for complexes in which the C-ter EF hand pair is Ca^{2+}-free are 30−100 times slower.

Dissociation of CaM in the Presence of CaM-Binding Peptides. We extended our analysis of the kinetics of native and mutant CaM−$BSCaM_{IQ}$ complexes by examining dissociation in the presence of a large molar excess of peptides based on the IQ domain in neurogranin (ngPEP) and the CaM-binding domain in CaM kinase II (ckPEP), which does not bind CaM with significant affinity in the absence of Ca^{2+}. In the presence of ngPEP, Ca^{2+}-free native CaM dissociates with an apparent rate constant of 0.8 ± 0.2 s^{-1} (Figure 2A), and essentially identical rate constants were derived for the Ca^{2+}-free complexes with the two mutant CaMs (data not shown). In the presence of ckPEP, Ca^{2+}-saturated NC_xCaM and N_xCCaM dissociate with rate constants of 30.2 ± 4.2 and 630.7 ± 16.4 s^{-1} (Figure 2B,D). These values agree with those derived from replots of k_{obs} *vs* [CaM] (Table 1). In contrast, Ca^{2+}-saturated native CaM dissociates with an apparent rate constant of 565.1 ± 13.1 s^{-1} in the presence of ckPEP (Figure 2C), which is ~10-fold faster than the rate derived from a replot of k_{obs} *vs* [CaM] (Table 1). The accelerated dissociation rate observed in the presence of ckPEP indicates that dissociation occurs via a ternary complex between ckPEP, CaM, and $BSCaM_{IQ}$. Since the measured fluorescence time course is monophasic and has an amplitude consistent with formation of free $BSCaM_{IQ}$, formation of the ternary complex itself does not appear to be associated with a significant change in fluorescence. However, it is conceivable that the fluorescence time course corresponds with formation of the ternary complex itself, rather than dissociation of $BSCaM_{IQ}$. This is unlikely because the apparent dissociation rate does not exhibit a second-order dependence on the ckPEP concentration (data not shown).

Dissociation of Ca^{2+}. We have previously reported that under equilibrium conditions Ca^{2+} binding to the C-ter EF hand pair in the CaM−$BSCaM_{IQ}$ complex reduces the affinity of the complex, and subsequent binding to the N-ter EF hand pair raises it (*15*). The Ca^{2+}-binding affinity of the C-ter EF hand pair is thus reduced due to negative energy coupling, while the affinity of the N-ter pair is increased due to positive energy coupling (*15*). To investigate the mechanistic basis for these changes in Ca^{2+}-binding affinity, we determined Ca^{2+} dissociation rates for free and bound native and mutant CaMs. In general agreement with others (*19*, *24*−*27*), Ca^{2+} was found to dissociate from the C-ter and N-ter EF hand pairs in free CaM with rate constants of 10.3 ± 0.7 and 1152 ± 117 s^{-1}. It is important to note that dissociation rate constants were determined for free CaM using a 5 μL observation cell, rather than the standard 20 μL cell. This reduces the dead time of the stopped-flow fluorometer to below 1 ms, allowing this fast rate to be measured. Unfortunately, efficient rapid mixing was not obtained when we attempted to use the smaller cell with solutions containing $BSCaM_{IQ}$, presumably due to their

Table 1: Association and Dissociation Rate Constants for Native and Mutant CaM−$BSCaM_{IQ}$ Complexes[a]

	k_{obs} *vs* [CaM] plot		k_{off}/k_{on}	equil	peptide trap
CaM	k_{on} (M^{-1} s^{-1})	k_{off} (s^{-1})	K_d (μM)	K_d (μM)	k_{off} (s^{-1})
NC	$3.6 \pm 0.2 \times 10^5$	0.9 ± 0.2	2.5 ± 0.6	2.3 ± 0.1	0.8 ± 0.2
N_xC	$3.9 \pm 0.6 \times 10^5$	1.1 ± 0.3	2.8 ± 0.7	2.1 ± 0.2	0.9 ± 0.2
NC_x	$2.9 \pm 0.5 \times 10^5$	0.9 ± 0.2	3.1 ± 0.9	2.5 ± 0.3	0.7 ± 0.3
N_xC_2	$4.1 \pm 0.2 \times 10^7$	558.8 ± 10.1	13.6 ± 1.1	14.4 ± 1.3	630.7 ± 16.4
N_2C_x	$1.1 \pm 0.2 \times 10^6$	30.9 ± 1.6	28.1 ± 5.3	36.7 ± 3.9	30.2 ± 4.2
N_2C_2	$3.1 \pm 0.2 \times 10^7$	69.4 ± 9.6	2.2 ± 0.3	2.5 ± 0.1	565.1 ± 13.1

[a] The first two columns contain k_{on} and k_{off} values derived from linear least-squares fits to replots of k_{obs} *vs* [CaM] (see Figure 1). K_d values calculated using these rate constants are consistent with previously determined equilibrium K_d values (*15*). The last column contains k_{off} values derived from dissociation time courses measured in the presence of large molar excesses of ngPEP or ckPEP (see Figure 2).

Table 2: Ca^{2+} Association and Dissociation Rate Constants for Native and Mutant CaMs Free in Solution or Bound to $BSCaM_{IQ}$[a]

	N-ter EF hand pair		C-ter EF hand pair	
	k_{on} (M^{-1} s^{-1})	k_{off} (s^{-1})	k_{on} (M^{-1} s^{-1})	k_{off} (s^{-1})
CaM				
NC	$3.1 \pm 1.2 \times 10^{8\,A}$	1152 ± 117^B	$3.4 \pm 2.4 \times 10^{7\,A}$	10.3 ± 0.7
N_xC	na	na	$5.8 \pm 3.2 \times 10^{7\,A}$	10.8 ± 0.6
NC_x	$3.4 \pm 1.5 \times 10^{8\,A}$	1298 ± 135^B	na	na
CaM−$BSCaM_{IQ}$				
NC	$3.0 \pm 1.2 \times 10^{8\,A}$	473.4 ± 37.9 (528.3 ± 3.3)	$3.2 \pm 0.1 \pm 10^6$	11.7 ± 0.5 (13.5 ± 0.1)
N_xC	na	na	$3.1 \pm 0.1 \pm 10^6$	11.8 ± 0.5
NC_x	nd	nd	na	na

[a] Ca^{2+} binding was modeled according to a sequential mechanism with a rapidly equilibrating first step (Scheme 1), so these rate constants correspond with the second Ca^{2+}-binding step. Values indicated by na are not applicable; those indicated by nd are too fast to measure in the stopped-flow fluorometer, which has a dead-time of ~1.4 ms. Association rate constants (k_{on}) designated by a superscript "A" were calculated using the dissociation rate constants (k_{off}) given in this table and previously determined equilibrium constants for the second Ca^{2+} binding step (*15*). Association rate constants for the C-ter EF hand pair in the CaM−$BSCaM_{IQ}$ complex were derived from a global analysis of the fluorescence time courses presented in Figure 5. k_{off} values designated by a superscript "B" were determined using a 5 μL observation cell, which reduces the stopped-flow dead time to below 1 ms, but unfortunately cannot be used with solutions containing $BSCaM_{IQ}$ due to their higher viscosity. k_{off} values for the CaM−$BSCaM_{IQ}$ complex given in parentheses were derived from a global analysis of the fluorescence time courses presented in Figure 4. All other k_{off} values were derived from quin-2 fluorescence data (Figure 3).

higher viscosities. Dissociation rate constants of 11.7 ± 0.5 s^{-1} and 473.4 ± 37.9 s^{-1} were derived when CaM is bound to $BSCaM_{IQ}$ (Figure 3A). To confirm that the slower rate constant corresponds with the C-ter EF hand pair, dissociation rate constants were derived for N_xCCaM in the presence and absence of $BSCaM_{IQ}$ (Figure 3B), and respective values of 11.8 ± 0.5 and 10.8 ± 0.6 s^{-1} were obtained. The dissociation rate constant of 473.4 ± 37.9 s^{-1} derived for the native CaM complex therefore corresponds with the N-ter EF hand pair, and the slower rate corresponds with the C-ter pair. The increased Ca^{2+}-binding affinity of the N-ter sites in the CaM−$BSCaM_{IQ}$ complex is thus correlated with a decrease in the dissociation rate for Ca^{2+}. The reduced affinity of the C-ter pair of sites does not appear to involve a change in the Ca^{2+} dissociation rate. Determination of a Ca^{2+} dissociation rate for the NC_xCaM−$BSCaM_{IQ}$ complex, which exhibits negative energy coupling (*15*), was not possible because maintenance of the complex requires $BSCaM_{IQ}$ solutions with viscosities that preclude efficient mixing.

The Transition from Ca^{2+}-Saturated to Ca^{2+}-Free Complex. Having determined binding kinetics and Ca^{2+} dissociation rates for mutant and native CaM−$BSCaM_{IQ}$ complexes, we next analyzed the fluorescence changes associated with the transition from the Ca^{2+}-saturated to the Ca^{2+}-free complex. Fluorescence time courses were measured after addition of a large molar excess of BAPTA to the Ca^{2+}-saturated CaM−$BSCaM_{IQ}$ complex (Figure 4A,B). Individual time courses measured on different time scales are offset in the figure for presentation purposes. These data were globally fitted to the kinetic model presented in Scheme 2. In this model Ca^{2+} dissociates sequentially from the N-ter and C-ter EF hand pairs because the N-ter sites have much faster kinetics. Relative molar fluorescence amplitudes were assigned to all kinetic species as detailed in Materials and Methods. The fitted curves presented in the figure were generated by varying only k'_{-2} and k'_{-4}, the Ca^{2+} dissociation rate constants for N-ter and C-ter EF hand pairs in bound CaM. All other necessary parameters were fixed to the values given in Tables 1 and 2. Parameter values derived for N_x-CCaM were applied to the intermediate species in which Ca^{2+} remains bound to the C-ter EF hand pair (NC_2−B). Rate constants for "fast" steps were arbitrarily assigned values 10-fold higher than the rate constants for the steps preceding them. The rising phase in fluorescence corresponds largely with formation and dissociation of the NC_2−B intermediate, although dissociation of the initial Ca^{2+}-saturated complex due to dilution also contributes. The falling phase corresponds with formation of the final Ca^{2+}-free complex, which is not as fluorescent as the initial complex. The slight discrepancy between the fitted curves and the data measured during the first few milliseconds is probably due to the simplifying assumption that short-lived intermediates with Ca^{2+} bound to only a single site in an EF hand pair are effectively nondissociating (dashed arrows in Scheme 2). The overall quality of the fit suggests that this scheme nevertheless represents a reasonable minimal model. The validity of the model is lent further support by the fact that fitted values of 13.5 ± 0.1 and 528.3 ± 3.3 s^{-1} were derived for k'_{-2} and k'_{-4}, which are essentially identical to the Ca^{2+}-dissociation

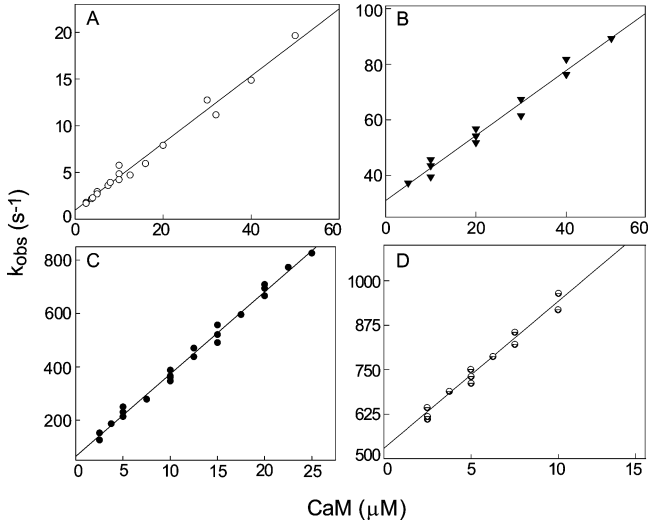

FIGURE 1: Association of native and mutant CaMs with $BSCaM_{IQ}$. Values for k_{obs} were derived from monoexponential fits to time courses for $BSCaM_{IQ}$ fluorescence measured after addition of CaM. The lowest final CaM concentration produced was in all cases at least 5-fold greater than final $BSCaM_{IQ}$ concentration. Pseudo-first-order conditions were thus maintained so that $k_{obs} = k_{on}[CaM] + k_{off}$. (A) Replot of k_{obs} values determined in the absence of Ca^{2+} *vs* the concentration of CaM. Nominally Ca^{2+}-free conditions were produced by including 3 mM BAPTA in all experimental buffers. The k_{on} and k_{off} values derived from the linear fit shown are $3.6 \pm 0.2 \times 10^5$ M^{-1} s^{-1} and 0.9 ± 0.2 s^{-1}. k_{on} and k_{off} values derived for Ca^{2+}-free N_xCCaM are $3.2 \pm 0.1 \times 10^5$ M^{-1} s^{-1} and 1.1 ± 0.1 s^{-1}, and values of $2.9 \pm 0.1 \times 10^5$ M^{-1} s^{-1} and 0.7 ± 0.1 s^{-1} were derived for Ca^{2+}-free NC_xCaM (data not shown). (B) Replot of k_{obs} values determined in the presence of 250 μM $CaCl_2$ *vs* the concentration of NC_xCaM. The k_{on} and k_{off} values derived from the linear fit shown are $1.1 \pm 0.2 \times 10^6$ M^{-1} s^{-1} and 30.9 ± 1.6 s^{-1}. (C) Replot of k_{obs} values determined in the presence of 250 μM $CaCl_2$ *vs* the concentration of native CaM. The k_{on} and k_{off} values derived from the linear fit shown are $3.1 \pm 0.2 \times 10^7$ M^{-1} s^{-1} and 69.4 ± 9.6 s^{-1}. (D) Replot of k_{obs} values determined in the presence of 250 μM $CaCl_2$ *vs* the N_xCCaM concentration. k_{on} and k_{off} values of $4.1 \pm 0.2 \times 10^7$ M^{-1} s^{-1} and 558.8 ± 10.1 s^{-1} were derived from linear fit shown.

rate constants derived from Ca^{2+} trapping experiments (Table 2).

Ca^{2+}-Dependent Release of CaM in the Presence of a CaM-Binding Peptide. Given the hypothesis that neuromodulin participates in CaM storage and delivery (*9*, *28*, *29*), we were particularly interested in investigating release of CaM from the neuromodulin IQ domain in the presence of Ca^{2+} and a peptide (ckPEP) based on the CaM-binding domain in CaM kinase II, an abundant enzyme in neurons (*30*). From an experimental standpoint, analysis of this process is complicated by the fact that two pathways for sequential occupancy of the N-ter and C-ter EF hand pairs must be considered (see Scheme 3). We therefore initially analyzed the behavior of the $N_xCCaM-BSCaM_{IQ}$ complex to eliminate the contribution of the N-ter pair of Ca^{2+} binding sites.

Fluorescence time courses measured after adding excess ckPEP and different amounts of Ca^{2+} to the Ca^{2+}-free mutant complex are presented in Figure 5A. These data were globally fitted according the steps in Scheme 3 that correspond with formation and dissociation of the intermediate NC_2-B complex. The second Ca^{2+}-binding step is effectively irreversible because Ca^{2+} dissociates from the NC_2-B complex at a rate of ~ 10 s^{-1}, while the complex itself

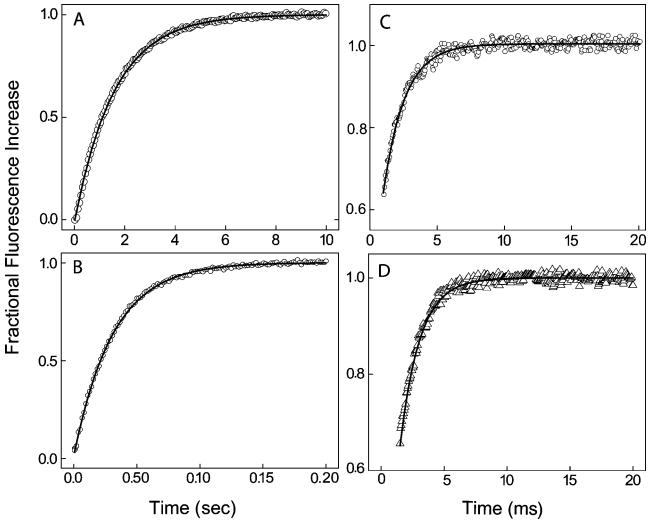

FIGURE 2: Dissociation of complexes between native and mutant CaMs and $BSCaM_{IQ}$ in the presence of CaM-binding peptides. In all cases a range of peptide concentrations was investigated to ensure that a concentration sufficient to prevent rebinding of CaM was used. (A) Dissociation of the Ca^{2+}-free $CaM-BSCaM_{IQ}$ complex after addition of a peptide (ngPEP) based on the CaM-binding domain in neurogranin. Nominally Ca^{2+}-free conditions were produced by including 3 mM BAPTA in all experimental buffers. The final $BSCaM_{IQ}$ and CaM concentrations were 10 and 1 μM; the final peptide concentration was 100 μM. The k_{off} value derived from monoexponential fits to these and similar data is 0.8 ± 0.2 s^{-1}. (B**)** Dissociation of the $NC_xCaM-BSCaM_{IQ}$ complex in the presence of 250 μM $CaCl_2$ after addition of a peptide (ckPEP) based on the CaM-binding domain in CaM kinase II. The final $BSCaM_{IQ}$ and N_xCCaM concentrations were 50 and 10 μM; the final ckPEP concentration was 100 μM. The dissociation rate constant derived from fits of these and similar data to single exponentials is 30.2 ± 4.2 s^{-1}. **(**C**)** Dissociation of $CaM-BSCaM_{IQ}$ complex in the presence of 250 μM $CaCl_2$ after addition of ckPEP at a final concentration of 100 μM. The final $BSCaM_{IQ}$ and CaM concentrations were 12.5 and 2.5 μM. The apparent dissociation rate constant derived from fits to these and similar data to single exponentials is 565.1 ± 13.1 s^{-1}. **(**D**)** Dissociation of the Ca^{2+}-saturated $N_xCCaM-BSCaM_{IQ}$ complex in the presence of 250 μM $CaCl_2$ after addition of ckPEP at a final concentration of 100 μM. The final $BSCaM_{IQ}$ and N_xCCaM concentrations were 25 and 5 μM. The apparent dissociation rate constant derived from fits of these and similar data to single exponentials is 630.7 ± 16.4 s^{-1}.

dissociates at a rate of ~ 500 s^{-1} (Tables 1 and 2). The fit presented in panel A was produced by varying the dissociation constant (K_1) for the first C-ter Ca^{2+}-binding step and the association rate constant (k_2) for the second Ca^{2+}-binding step. The other necessary parameter was the dissociation rate constant for the NC_2-B intermediate (k_{-NC_2}), which was fixed to the value given in Table 2. Dissociation of this intermediate is effectively irreversible, as there is a large molar excess of ckPEP. Relative molar fluorescence amplitudes were assigned to all kinetic species as detailed in Materials and Methods. The observed increases in fluorescence reflect the increase that occurs when the NC_2-B intermediate forms, and the further increase that occurs when it dissociates. The quality of the fit suggests that a three step kinetic model is a reasonable minimal description of this process. The fitted values obtained for K_1 and k_2 are 4.8 ± 0.9 μM and $3.1 \pm 0.1 \times 10^6$ M^{-1} s^{-1}. The latter value is $\sim$10-fold less than the Ca^{2+} association rate constant estimated for free CaM (Table 2).

We next measured a series of fluorescence time courses for the native $CaM-BSCaM_{IQ}$ complex using the same

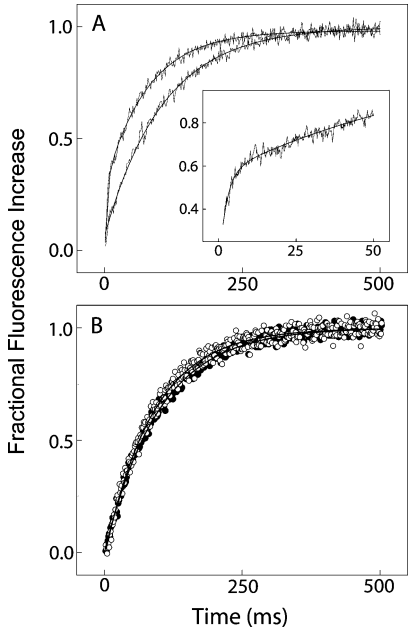

FIGURE 3: Dissociation of Ca^{2+} from the complex between $BSCaM_{IQ}$ and CaM or N_xCCaM. The fluorescent Ca^{2+} chelator quin-2 was used as a Ca^{2+} trap. Dissociation of Ca^{2+} from native or mutant CaM therefore corresponds directly with a Ca^{2+}-dependent increase in quin-2 fluorescence. A range of quin-2 concentrations was investigated to ensure that a concentration sufficient to prevent rebinding of Ca^{2+} was used. (A) Dissociation of Ca^{2+} from free CaM (lower trace) and from the CaM−$BSCaM_{IQ}$ complex (upper trace). The quin-2 fluorescence time course for Ca^{2+} dissociation from free CaM was generated by mixing a solution containing 4 μM CaM and 50 μM $CaCl_2$ with an equal volume of 400 μM quin-2. These data are fitted by a single exponential with a rate constant of 10.3 ± 0.7 s^{-1} and an amplitude corresponding with dissociation of ~2 Ca^{2+} ions. Dissociation of two additional Ca^{2+} ions occurred within the instrument dead time. The quin-2 fluorescence time course for Ca^{2+} dissociation from the CaM−$BSCaM_{IQ}$ complex was generated by mixing a solution containing 25 μM $BSCaM_{IQ}$, 4 μM CaM, and 50 μM $CaCl_2$ with an equal volume of 400 μM quin-2. The data presented are fitted by a double exponential. The slower process has an apparent rate constant of 14.7 ± 0.5 s^{-1} and an amplitude corresponding with dissociation of ~2 Ca^{2+} ions. The faster rate was derived from data measured over a shorter time interval (inset). These data are fitted by a double exponential with rate constants of 427.4 ± 35 and 11.7 ± 0.5 s^{-1}, and respective amplitudes corresponding with dissociation of ~1.5 and ~2 Ca^{2+} ions. If the faster process is forced to have an amplitude corresponding with dissociation of 2 Ca^{2+} ions, then apparent rate constants of 473.4 ± 37.9 s^{-1} and 12.9 ± 0.7 s^{-1} are derived for the faster and slower processes. (B) Dissociation of Ca^{2+} from the N_xCCaM−$BSCaM_{IQ}$ complex (●) and from free N_xCCaM (○). For these experiments a solution containing 4 μM N_xCCaM and 50 μM $CaCl_2$ in the presence or absence of 25 μM $BSCaM_{IQ}$ was mixed with an equal volume of 400 μM quin-2. The two resulting quin-2 fluorescence time courses are essentially superimposable. Ca^{2+}-dissociation rate constants of 10.8 ± 0.6 s^{-1} and 11.8 ± 0.5 s^{-1} were derived for free and bound N_xCCaM from fits of these data to single exponentials with amplitudes corresponding to dissociation of ~2 Ca^{2+} ions.

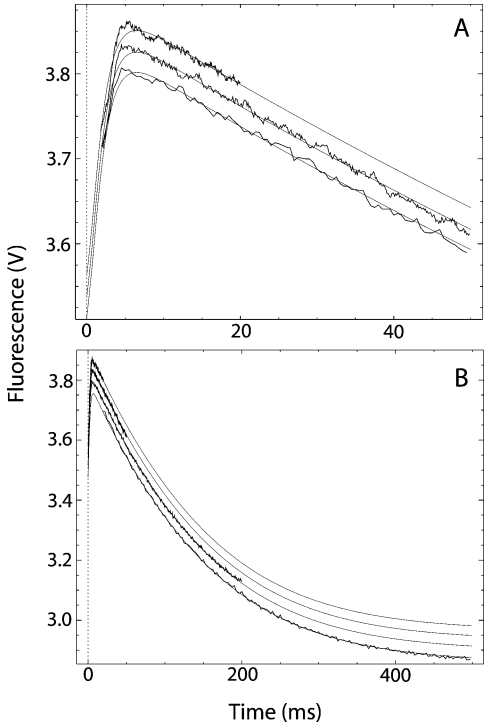

FIGURE 4: The transition from Ca^{2+}-saturated to Ca^{2+}-free CaM−$BSCaM_{IQ}$ complex. (A, B) Buffer containing 48 μM CaM and 4 μM $BSCaM_{IQ}$ in 500 μM $CaCl_2$ was rapidly mixed with an equal volume of buffer containing 10 mM BAPTA. Data measured over 20, 50, and 200 ms time intervals are presented in panels A and B. Data measured over a 500 ms time interval are included in panel B. The individual data sets are offset on the *y*-axis for presentation purposes. These data were globally fitted to the model presented in Scheme 2 by iteratively varying the values for k'_{-2} and k'_{-4}, the Ca^{2+} dissociation rate constants for bound CaM, using the DynaFit program (*18*). Relative molar fluorescence amplitudes were assigned to the various kinetic species as detailed in Materials and Methods. Association and dissociation rate constants applied to the various Ca^{2+}-bound forms of the CaM−$BSCaM_{IQ}$ complex are given in Table 1. Ca^{2+} dissociation rate constants applied to free CaM are given in Table 2. Parameters assigned to the NC_2−B species were determined using N_xCCaM. No attempt was made to include the standard errors associated with fixed parameter values. Steps marked as fast were arbitrarily assigned rates 10-fold faster than the steps preceding them. The fitted values obtained for k'_{-4} and k'_{-2} are 528.3 ± 3.3 and 13.5 ± 0.1 s^{-1}.

experimental approach (Figure 5B). These data were globally fitted according to the model depicted in Scheme 3. The rate constant for dissociation of the Ca^{2+} saturated CaM−$BSCaM_{IQ}$ complex in the presence of ckPEP is designated as $k^{T}_{N_2C_2}$, since this step appears to involve formation of a ternary complex with the peptide. The bracketed portion of the scheme can be omitted from fitting calculation without significant effect, apparently because in the presence of ckPEP the NC_2−B and N_2C_2−B intermediates dissociate at essentially the same rate (Table 2), and there is little difference in their fluorescence (*15*). Binding of Ca^{2+} to the N-ter EF hand pair prior to the C-ter pair is modeled as rapidly equilibrating because the rates at which N_2C−B dissociates or is converted to the N_2C_2-B intermediate are relatively slow (see Tables 1 and 2). The fit shown in Figure 5B was produced by varying only K'_1 and k'_2. Previously determined dissociation constants of 122 and 9.4 μM were assigned to K'_3 and K'_4 (*15*). Other required kinetic parameters, including K_1 and k_2, were fixed to the values given in Tables 1 and 2. The parameters for reactions involving NC_2−B and N_2C−B were derived using N_xCCaM and NC_x-CaM. Relative molar fluorescence amplitudes were assigned to all kinetic species as detailed in Materials and Methods. The observed fluorescence time courses reflect increases due to formation of the NC_2−B and N_2C−B intermediates, and to release of $BSCaM_{IQ}$ (B). Formation of the N_2C−B intermediate produces a fluorescence increase that occurs

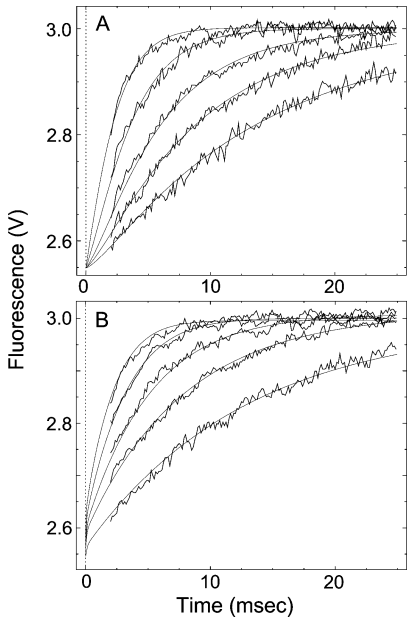

FIGURE 5: Dissociation of the initially Ca^{2+}-free complex between $BSCaM_{IQ}$ and native CaM or N_xCCaM after addition of Ca^{2+} and ckPEP. Fluorescence data were measured after adding a solution containing 200 μM ckPEP, along with $CaCl_2$ in amounts producing the specified final concentrations, to an equal volume of a decalcified solution containing 20 μM $BSCaM_{IQ}$ and either 4 μM native CaM or N_xCCaM. (A) Dissociation of the $N_xCCaM-BSCaM_{IQ}$ complex in the presence of ckPEP with Ca^{2+} at concentrations of 30, 45, 67.5, 125, or 250 μM (lowermost to uppermost trace). These data were globally fitted according to an abbreviated version of the model presented in Scheme 3 containing only the steps associated with formation and dissociation of NC_2-B. The fit shown was produced by iteratively varying the values for K_1 and k_2 using the DynaFit program (*18*). Relative molar fluorescence amplitudes were assigned to the various kinetic species as detailed in Materials and Methods. The dissociation rate constants assigned to the NC_2-B species are given in Table 1. The NC−B species is effectively nondissociating on this time scale. No attempt was made to include the standard errors associated with the fixed parameter values. The K_1 and k_2 values derived from the global fit shown are 4.6 ± 0.9 μM and 3.1 ± 0.1 × 10^6 M^{-1} s^{-1}. (B) Dissociation of the native $CaM-BSCaM_{IQ}$ complex in the presence of ckPEP with Ca^{2+} at a concentrations of 30, 45, 67.5, 125, or 250 μM (lowermost to uppermost trace). Fluorescence time courses were globally fitted according to the model presented in Scheme 3 by iteratively varying the values for K_1' and k_2' using the DynaFit program (*18*). Previously determined values of 122 and 9.4 μM were assigned to $K_3'$and K_4' (*15*). The dissociation rate constants assigned to the NC−B, N_2C-B, NC_2-B, and N_2C_2-B species are given in Table 1. The values used for the N_2C-B and NC_2-B species were determined using N_xCCaM and NC_xCaM. Values of 4.6 ± 0.9 μM and 3.1 ± 0.1 × 10^6 M^{-1} s^{-1} were assigned to K_1 and k_2 (Table 2). Relative molar fluorescence amplitudes were assigned to the various kinetic species as detailed in Materials and Methods. The K_1' and k_2' values derived from the global fit shown are 4.1 ± 0.6 μM and 3.2 ± 0.1 × 10^6 M^{-1} s^{-1}.

within the ~1.4 ms dead time of the stopped-flow (Figure 5B). This increase corresponds with rapidly equilibrating binding of Ca^{2+} to the N-ter EF hand pair, and its amplitude increases as a function of the free Ca^{2+} concentration in accordance with the values used for K_3' and K_4'. The amplitude of this phase is also linked to the amount of $BSCaM_{IQ}$ dissociation that occurs via the lower pathway in Scheme 3. Thus, at a free Ca^{2+} concentration of ~10 μM, dissociation via this pathway is negligible, while at a free Ca^{2+} concentration of ~70 μM dissociation via the upper and lower pathways is equivalent (data not shown). At a free Ca^{2+} concentration of 250 μM the proportion of dissociation via the lower pathway saturates at a value of ~65%. This occurs in spite of the much faster Ca^{2+}-binding kinetics of the N-ter EF hand pair because the N_2C-B intermediate dissociates relatively slowly. The overall quality of the fit indicates that Scheme 3 is an acceptable minimal model. Fitted values of 4.1 ± 0.6 μM and 3.2 ± 0.1 × 10^6 M^{-1} s^{-1} were derived for K_1' and k_2', which are not significantly different from the values derived for K_1 and k_2. The association rate constant for the C-ter Ca^{2+}-binding sites in CaM therefore appears to be reduced to the same extent, regardless of whether Ca^{2+} is bound to the N-ter pair of sites.

DISCUSSION

In this paper we present the results of a kinetic analysis of the complex between CaM and $BSCaM_{IQ}$, a fluorescent reporter containing the IQ domain from neuromodulin (*15*). Association and dissociation rate constants for various Ca^{2+}-bound forms of the complex were determined, as well as many of the rate constants governing Ca^{2+} binding to the complex. Kinetic models incorporating these rate constants were developed that account for the $BSCaM_{IQ}$ fluorescence responses observed when Ca^{2+} is removed from the Ca^{2+}-saturated complex or when Ca^{2+} is added to the Ca^{2+}-free complex in the presence of a peptide based on the CaM-binding domain in CaM kinase II. Three key points are evident: (1) Association and dissociation of the complex is accelerated in the presence of Ca^{2+}. (2) When CaM is bound to the IQ domain, the Ca^{2+}-association rate constant for the C-ter EF hand pair is reduced ~10-fold and the Ca^{2+}-dissociation rate constant for the N-ter EF hand pair is reduced ~3-fold. (3) Ca^{2+}-saturated CaM can be transferred from the neuromodulin IQ domain to canonical CaM-binding domains, such as the one in CaM kinase II, via an intermediate ternary complex.

CaM-Binding Kinetics. As seen in Table 1, there is complete agreement between the association and dissociation rate constants for various native and mutant $CaM-BSCaM_{IQ}$ complexes derived from replots of k_{obs} *vs* [CaM] and the corresponding equilibrium K_d values. The association and dissociation rates for the Ca^{2+}-saturated CaM−IQ domain complex and the C-ter Ca^{2+}-bound intermediate are 30- to 100-fold faster than for the Ca^{2+}-free complex (Table 1). The association rate constants derived for the Ca^{2+}-saturated complex and the C-ter Ca^{2+}-bound intermediate are similar to those derived for the Ca^{2+}-saturated complexes between CaM and other types of CaM-binding sequences (*22*, *23*, *31*). The kinetics of the N-ter Ca^{2+}-bound intermediate are comparatively slow, as its association rate constant is only 3-fold faster than the rate constant for the Ca^{2+}-free complex (Table 1). This indicates that slow binding kinetics are a feature of interactions between the Ca^{2+}-free C-ter CaM lobe and the IQ domain.

Dissociation rate constants were also determined for native and mutant $CaM-BSCaM_{IQ}$ complexes by using ckPEP or ngPEP to trap CaM. With only one exception, these values agree with those derived from replots of k_{obs} *vs* [CaM] (Table 1). The exception is the Ca^{2+}-saturated native CaM−

$BSCaM_{IQ}$ complex, which dissociates at a rate of 565.1 ± 13.1 in the presence of ckPEP, compared with a rate of 69.4 ± 9.6 derived from an analysis of binding kinetics (Table 1). Dissociation is accelerated in the presence of the peptide, since the slower rate is consistent with the K_d value for this complex (Table 1). The only reasonable explanation for this behavior is that in the presence of ckPEP dissociation occurs via a ternary complex between the peptide, CaM, and $BSCaM_{IQ}$. The absence of an effect of ckPEP on the dissociation rates for the intermediate CaM−$BSCaM_{IQ}$ complexes in which Ca^{2+} is bound only to the N-ter or C-ter EF hand pair suggests that neither can participate in a ternary complex, or that they do so with no apparent effect on their kinetic properties. Gaertner and co-workers have previously presented evidence consistent with formation of a ternary complex between intact CaM kinase II, CaM, and the IQ domain in neurogranin (*32*). A ternary complex intermediate provides a route for efficient delivery of CaM from neuromodulin to other CaM-binding proteins, consistent with its proposed role in CaM storage and delivery.

Ca^{2+}-Binding Kinetics. Ca^{2+} dissociation rates for the N-ter and C-ter EF hand pairs in bound native and mutant CaMs were directly evaluated in Ca^{2+} trapping experiments (Table 2). These rates agree with those derived from a global analysis of $BSCaM_{IQ}$ fluorescence data measured during the transition from the Ca^{2+}-saturated to the Ca^{2+}-free complex (Figure 4A,B; Table 2). The dissociation rate derived for the N-ter EF hand pair in bound CaM (k'_{-4}) is 473.4 ± 37.9 s^{-1}, while the corresponding value for free CaM (k_{-4}) is 1298 ± 135 s^{-1}. In principle, the k_{-4}/k'_{-4} ratio of 2.7 ± 0.4 should be comparable to the K_4/K'_4 ratio, but in practice the individual dissociation constants for an EF hand pair are not as well determined as the product of the constants (*15*). It is therefore preferable to compare the $K_3K_4/K'_3K'_4$ ratio with the square of the k_{-4}/k'_{-4} ratio. The latter ratio is squared because k_{-4} and k'_{-4} both correspond with dissociation of two Ca^{2+} ions (see Scheme 2). The value of 10.2 ± 1.8 derived for $K_3K_4/K'_3K'_4$ from data published previously is in reasonable agreement with the square of k_{-4}/k'_{-4}, which is 7.3 ± 1.1 (*15*). This suggests that the increased Ca^{2+}-binding affinity of the N-ter EF hand pair in the CaM−IQ domain complex is due to a decreased Ca^{2+} dissociation rate. The Ca^{2+} dissociation rates determined for the C-ter EF hand pair in bound and free CaM are essentially identical (Table 2), so the reduced affinity of these sites in the CaM−IQ domain complex is not due to an accelerated dissociation rate.

Association rates for Ca^{2+} were derived for the C-ter EF hand pair in bound CaM from a global analysis of fluorescence data measured after addition of Ca^{2+} and ckPEP to the Ca^{2+}-free native or N_xCCaM complex with $BSCaM_{IQ}$ (Figure 5A,B; Table 2). Association rates could not be determined for the N-ter EF hand pair. Since essentially the same kinetic parameters were derived for the C-ter EF hand pairs in the native and N_xCCaM complexes with $BSCaM_{IQ}$, we shall only discuss our analysis of the latter in detail. We have modeled Ca^{2+} binding to an EF hand pair as a sequential process, with a rapidly equilibrating first step and a slower second step. Fitted values of 4.6 ± 0.9 μM and 3.1 ± 0.1 × 10^6 M^{-1} s^{-1} were derived for K_1, the dissociation constant for the first step, and k_2, the association rate constant for the second step. In the presence of ckPEP, we can ignore k_{-2}, the rate constant for reversal of the second step, because Ca^{2+} dissociates ~50-fold slower from the complex than does Ca^{2+}-saturated N_xCCaM, which is then trapped by ckPEP (Table 1). The value derived for k_2 is ~10-fold less than the corresponding value for free N_xCCaM (Table 2). By combining the values we have derived for K_1 and k_2 with a k_{-2} value of 11.8 ± 0.5 (Table 2), we can calculate a value of 18.2 ± 5.1 μM^2 for the product of the two Ca^{2+} dissociation constants for the $N_xCCaM-BSCaM_{IQ}$ complex. This is in reasonable agreement with the value of 24.6 ± 2.7 μM^2 derived from equilibrium Ca^{2+}-binding data (*15*). Thus, the reduced affinity of the C-ter EF hand pair in bound CaM appears to be due to a reduced Ca^{2+} association rate, as expected given the absence of any effect on the dissociation rate.

A surprising aspect of our results is that the same association rate constant is derived for Ca^{2+} binding to the C-ter EF hand pair, regardless of whether the N-ter EF hand pair is occupied by Ca^{2+}. Since the affinity of C-ter EF hand pair for Ca^{2+} is higher when the N-ter sites are occupied, it appears that the dissociation rate constant must be reduced to account for this (*15*). This is difficult to prove because Ca^{2+} dissociates from the C-ter sites much more slowly than it does from the N-ter sites. Thus, dissociation from the C-ter sites while the N-ter sites remain occupied cannot be observed in Ca^{2+} trapping experiments.

Implications for Neuromodulin Function. We have shown previously that under equilibrium conditions the apparent dissociation constant for the neuromodulin CaM−IQ domain complex has a bell-shaped dependence on the free Ca^{2+} concentration, peaking at a concentration of ~6 μM (*15*). Thus, release of CaM is promoted over a relatively narrow range of free Ca^{2+} concentrations. During a Ca^{2+} transient in a neuron the free Ca^{2+} concentration is likely to pass rapidly through this range, so we have proposed that release of CaM is only promoted briefly (*15*). Although the bell-shaped response curve has important implications with regard to regulation via CaM−IQ domain switches under equilibrium or quasi-equilibrium conditions, the analysis presented in this paper suggests some modifications to our understanding of what occurs during a rapid Ca^{2+} transient. The overall picture that emerges is one in which neuromodulin continuously maintains a local store of CaM that is efficiently delivered to target proteins in its Ca^{2+}-bound form during a Ca^{2+} transient.

The principal difference between the equilibrium and transient behaviors of the CaM−IQ domain complex is that the N-ter Ca^{2+}-bound intermediate plays a significant role when Ca^{2+} is rapidly increased to levels above 10 μM, as can occur locally during a neuronal Ca^{2+} transient (*33*−*38*). This intermediate does not form to a significant extent under equilibrium conditions, primarily because the C-ter Ca^{2+}-binding sites, although slower kinetically, have an EC50-(Ca^{2+}) of ~5 μM, while the value for the N-ter sites is ~35 μM (*15*). The N-ter Ca^{2+} bound intermediate dissociates at a relatively slow rate of ~30 s^{-1}, compared with a rate of ~500 s^{-1} for the C-ter intermediate. The kinetic properties of the CaM−IQ domain complex therefore appear to inhibit release of CaM in its Ca^{2+} free and N-ter Ca^{2+} bound intermediate forms (Table 1). When the C-ter Ca^{2+}-bound CaM intermediate dissociates, it is presumably captured by target proteins and rapidly converted to Ca^{2+}-saturated CaM, given the essentially diffusion-limited Ca^{2+} association rate

constants for the N-ter EF hand pair (Table 2). If the N-ter Ca^{2+}-bound intermediate were to dissociate to a significant extent, it could have negative consequences. First, since at least some targets appear to capture CaM via its C-ter lobe, the N-ter Ca^{2+}-bound intermediate may simply not be bound in some cases (*39*). Second, if a target were to capture this intermediate, the relatively slow Ca^{2+} association rate constants for the C-ter EF hand pair could impose a significant delay on target activation (Table 2). An implication of the latter point is that during a Ca^{2+} transient an abundant localized store of CaM provides it in its Ca^{2+}-saturated and C-ter Ca^{2+}-bound intermediate forms fast enough to meet the speed requirements of neuronal signaling. Given high enough local Ca^{2+} and CaM concentrations, this could occur through simple mass action. The similar affinities of neuromodulin for Ca^{2+}-free and Ca^{2+}-saturated CaM may serve not only to minimize diffusional losses of CaM, as we have proposed previously, but also to promote continuous diffusional recruitment of CaM. The degree to which ternary complexes play a role in CaM delivery in neurons remains to be established, although they clearly have the potential to facilitate this process.

We are currently extending these investigations by analyzing how the CaM−IQ domain complex responds to synthetic Ca^{2+} transients. The kinetic aspects of the CaM−IQ domain complex that we have described are likely to have counterparts in systems that are functionally modulated by CaM−IQ domain switches, such as ion channels and unconventional myosins. A particular intriguing possibility is that ratio of the N-ter and C-ter Ca^{2+}-bound intermediates that is produced during a Ca^{2+} transient provides a mechanism for producing functional responses that depend upon the amplitude and speed of the transient.

REFERENCES

1. Yagi, K., Yazawa, M., Kakiuchi, S., Ohshima, M., and Uenishi, K. (1978) Identification of an activator protein for myosin light chain kinase as the Ca^{2+}-dependent modulator protein, *J. Biol. Chem. 253*, 1338−1340.
2. Bredt, D. S., and Snyder, S. H. (1990) Isolation of nitric oxide synthetase, a calmodulin-requiring enzyme, *Proc. Nat. Acad. Sci. U.S.A. 87*, 682−685.
3. Venema, R. C., Sayegh, H. S., Arnal, J. F., and Harrison, D. G. (1995) Role of the enzyme calmodulin-binding domain in membrane association and phospholipid inhibition of endothelial nitric oxide synthase, *J. Biol. Chem. 270*, 14705−14711.
4. Dabrowska, R., Sherry, J. M., Aromatorio, D. K., and Hartshorne, D. J. (1978) Modulator protein as a component of the myosin light chain kinase from chicken gizzard, *Biochemistry 17*, 253−258.
5. Jurado, L. A., Chockalingam, P. S., and Jarrett, H. W. (1999) Apocalmodulin, *Physiol. Rev. 79*, 661−682.
6. Bahler, M., and Rhoads, A. (2002) Calmodulin signaling via the IQ motif, *FEBS Lett. 513*, 107−113.
7. Saimi, Y., and Kung, C. (2002) Calmodulin as an ion channel subunit, *Annu. Rev. Physiol. 64*, 289−311.
8. Halling, D. B., Aracena-Parks, P., and Hamilton, S. L. (2006) Regulation of voltage-gated Ca2+ channels by calmodulin [republished from Sci STKE. 2005 Dec 20;2005(315):re15; PMID: 16369047], *Science's Stke [Electronic Resource]: Signal Transduction Knowledge Environment 2006*, er1.
9. Estep, R. P., Alexander, K. A., and Storm, D. R. (1990) Regulation of free calmodulin levels in neurons by neuromodulin: relationship to neuronal growth and regeneration, *Curr. Top. Cell. Regul. 31*, 161−180.
10. Tran, Q. K., Black, D. J., and Persechini, A. (2003) Intracellular coupling via limiting calmodulin, *J. Biol. Chem. 278*, 24247−24250.
11. Rakhilin, S. V., Olson, P. A., Nishi, A., Starkova, N. N., Fienberg, A. A., Nairn, A. C., Surmeier, D. J., and Greengard, P. (2004) A network of control mediated by regulator of calcium/calmodulin-dependent signaling, *Science 306*, 698−701.
12. Isotani, E., Zhi, G., Lau, K. S., Huang, J., Mizuno, Y., Persechini, A., Geguchadze, R., Kamm, K. E., and Stull, J. T. (2004) Real-time evaluation of myosin light chain kinase activation in smooth muscle tissues from a transgenic calmodulin-biosensor mouse, *Proc. Natl. Acad. Sci. U.S.A. 101*, 6279−6284.
13. Gnegy, M. E. (1995) Calmodulin: effects of cell stimuli and drugs on cellular activation, *Prog. Drug Res. 45*, 33−65.
14. Gerendasy, D. D., Herron, S. R., Watson, J. B., and Sutcliffe, J. G. (1994) Mutational and biophysical studies suggest RC3/neurogranin regulates calmodulin availability, *J. Biol. Chem. 269*, 22420−22426.
15. Black, D. J., Leonard, J., and Persechini, A. (2006) Biphasic Ca2+-dependent switching in a calmodulin-IQ domain complex, *Biochemistry 45*, 6987−6995.
16. Fruen, B. R., Black, D. J., Bloomquist, R. A., Bardy, J. M., Johnson, J. D., Louis, C. F., and Balog, E. M. (2003) Regulation of the RYR1 and RYR2 Ca2+ release channel isoforms by Ca2+-insensitive mutants of calmodulin, *Biochemistry 42*, 2740−2747.
17. Tang, W., Halling, D. B., Black, D. J., Pate, P., Zhang, J. Z., Pedersen, S., Altschuld, R. A., and Hamilton, S. L. (2003) Apocalmodulin and Ca2+ calmodulin-binding sites on the Ca-(V)1.2 channel, *Biophys. J. 85*, 1538−1547.
18. Kuzmic, P. (1996) Program DYNAFIT for the analysis of enzyme kinetic data: application to HIV proteinase, *Anal. Biochem. 237*, 260−273.
19. Forsén, S., Vogel, H. J., and Drakenberg, T. (1986) Biophysical studies of calmodulin, in *Calcium and Cell Function* (Cheung, W. Y., Ed.) pp 113−157, Academic Press, New York.
20. Persechini, A., White, H. D., and Gansz, K. J. (1996) Different Mechanisms For Ca^{2+} Dissociation From Complexes of Calmodulin With Nitric Oxide Synthase or Myosin Light Chain Kinase, *J. Biol. Chem. 271*, 62−67.
21. Malmendal, A., Evenas, J., Forsen, S., and Akke, M. (1999) Structural dynamics in the C-terminal domain of calmodulin at low calcium levels, *J. Mol. Biol. 293*, 883−899.
22. Bowman, B. F., Peterson, J. A., and Stull, J. T. (1992) Pre-steady-state Kinetics of Activation of Rabbit Skeletal Muscle Myosin Light Chain Kinase by Ca^{2+}/Calmodulin, *J. Biol. Chem. 267*, 5346−5345.
23. Kasturi, R., Vasulka, C., and Johnson, J. D. (1993) Ca^{2+}, caldesmon, and myosin light chain kinase exchange with calmodulin, *J. Biol. Chem. 268*, 7958−7964.
24. Bayley, P., Ahlstrom, P., Martin, S. R., and Forsén, S. (1984) The kinetics of calcium binding to calmodulin: Quin 2 and Ans stopped-flow fluorescence studies, *Biochem. Biophys. Res. Commun. 120*, 185−191.
25. Martin, S. R., Teleman, A. A., Bayley, P. M., Drakenberg, T., and Forsén, S. (1985) Kinetics of calcium dissociation from calmodulin and its tryptic fragments. A stopped-flow fluorescence study using Quin 2 reveals a two-domain structure, *Eur. J. Biochem. 151*, 543−550.
26. Martin, S. R., Linse, S., Bayley, P. M., and Forsen, S. (1986) Kinetics of cadmium and terbium dissociation from calmodulin and its tryptic fragments, *Eur. J. Biochem. 161*, 595−601.
27. Johnson, J. D., Snyder, C., Walsh, M., and Flynn, M. (1996) Effects of myosin light chain kinase and peptides on Ca2+ exchange with the N- and C-terminal Ca2+ binding sites of calmodulin, *J. Biol. Chem. 271*, 761−767.
28. Chapman, E. R., Au, D., Alexander, K. A., Nicolson, T. A., and Storm, D. R. (1991) Characterization of the calmodulin binding domain of neuromodulin. Functional significance of serine 41 and phenylalanine 42, *J. Biol. Chem. 266*, 207−213.
29. Liu, Y. C., and Storm, D. R. (1990) Regulation of free calmodulin levels by neuromodulin: neuron growth and regeneration, *Trends Pharmacol. Sci. 11*, 107−111.
30. Nairn, A. C., and Picciotto, M. R. (1994) Calcium/calmodulin-dependent protein kinases, *Semin. Cancer Biol. 5*, 295−303.
31. Johnson, J. D., Holroyde, M. J., Crouch, T. H., Solaro, R. J., and Potter, J. D. (1981) Fluorescence studies of the interaction of calmodulin with myosin light chain kinase, *J. Biol. Chem. 256*, 12194−12198.

32. Gaertner, T. R., Putkey, J. A., and Waxham, M. N. (2004) RC3/neurogranin and Ca2+/calmodulin-dependent protein kinase II produce opposing effects on the affinity of calmodulin for calcium, *J. Biol. Chem. 279*, 39374−39382.
33. Etter, E. F., Minta, A., Poenie, M., and Fay, F. S. (1996) Near-membrane [Ca^{2+}] transients resolved using the Ca^{2+} indicator FFP18, *Proc. Natl. Acad. Sci. U.S.A. 93*, 5368−5373.
34. Marsault, R., Murgia, M., Pozzan, T., and Rizzuto, R. (1997) Domains of high Ca^{2+} beneath the plasma membrane of living A7r5 cells, *EMBO J. 16*, 1575−1581.
35. Davies, E. V., and Hallett, M. B. (1998) High micromolar Ca^{2+} beneath the plasma membrane in stimulated neutrophils, *Biochem. Biophys. Res. Commun. 248*, 679−683.
36. Klingauf, J., and Neher, E. (1997) Modeling Buffered Ca^{2+} Diffusion Near the Membrane—Implications For Secretion In Neuroendocrine Cells, *Biophys. J. 72*, 674−690.
37. Simon, S. M., and Llinas, R. R. (1985) Compartmentalization of the submembrane calcium activity during calcium influx and its significance in transmitter release, *Biophys. J. 48*, 485−498.
38. Llinas, R., and Moreno, H. (1998) Local Ca^{2+} signaling in neurons, *Cell Calcium 24*, 359−366.
39. Persechini, A., McMillan, K., and Leakey, P. (1994) Activation of myosin light chain kinase and nitric oxide synthase activities by calmodulin fragments, *J. Biol. Chem. 269*, 16148−16154.

BI700774S